

Article

Proposal of a System to Identify Failures and Evaluate the Efficiency of Internal Combustion Engines of Thermal Power Plants

Lilia Carneiro Ramos ¹, Frederico de Oliveira Assuncao ¹, Helcio Francisco Villa-Nova ², Germano Lambert-Torres ¹ , Erik Leandro Bonaldi ¹, Levy Ely de Lacerda de Oliveira ¹, Wilson Cesar Sant'Ana ^{2,*} , Ronny Francis Ribeiro Junior ¹ , Carlos Eduardo Teixeira ¹ and Paulo Germano Pinto de Medeiros ³

¹ Gnarus Institute, Itajuba 37500-052, MG, Brazil

² Pro-Reitoria de Pesquisa e Pos-Graduacao (PRPPG), Federal University of Itajuba, Itajuba 37500-903, MG, Brazil

³ Usina Termelétrica Pernambuco III S.A., Igarassu 53670-000, PE, Brazil

* Correspondence: wilson_santana@ieee.org



Citation: Ramos, L.C.; Assuncao, F.d.O.; Villa-Nova, H.F.; Lambert-Torres, G.; Bonaldi, E.L.; Oliveira, L.E.d.L.d.; Sant'Ana, W.C.; Ribeiro Junior, R.F.; Teixeira, C.E.; de Medeiros, P.G.P. Proposal of a System to Identify Failures and Evaluate the Efficiency of Internal Combustion Engines of Thermal Power Plants. *Energies* **2022**, *15*, 9047. <https://doi.org/10.3390/en15239047>

Academic Editor: Andrzej Teodorczyk

Received: 20 October 2022

Accepted: 23 November 2022

Published: 29 November 2022

Publisher's Note: MDPI stays neutral with regard to jurisdictional claims in published maps and institutional affiliations.



Copyright: © 2022 by the authors. Licensee MDPI, Basel, Switzerland. This article is an open access article distributed under the terms and conditions of the Creative Commons Attribution (CC BY) license (<https://creativecommons.org/licenses/by/4.0/>).

Abstract: Thermoelectric plants are one of the main forms of energy generation in the world, being the second main source of generation in Brazil. However, with rising fuel costs and greater concern for the environment, controlling the efficiency levels of these plants has become critical. This work presents a system to identify failures and evaluate the efficiency of internal combustion engines used in thermal power plants. To assess efficiency, the developed system monitors subsystem losses (such as cooling, lubrication, turbocharger, etc.). In addition, sensors for cylinder pressure and instantaneous speed were installed and comprise an online monitoring system for the pressure condition of each cylinder of the engines. All this is combined into a supervisory system that presents the Sankey diagram of the engine as its main information online and remotely. To validate the system, experiments were carried out in a controlled configuration (where faults were purposely inserted) and in a Brazilian thermal power plant. The results show that by using in-cylinder pressure and the WOIS database, it was possible to detect the presence of a fault as well as pinpoint its location.

Keywords: thermal efficiency; internal combustion engine; monitoring

1. Introduction

Despite the historical high penetration of renewable energy sources, since the 1990s, the Brazilian energy mix has shown a growth in Thermal Power Plants (TPP) based on fossil fuels [1]. According to the Brazilian regulatory agency for energy (ANEEL) [2], the granted electrical power to fossil fuels is approximately 35 GW (representing about 16% of the Brazilian energy mix) [3], which has been updated in 2022 to 45 GW (25%) [2].

One survey shows that almost 60% of the primary energy consumed by the industry (worldwide) is lost as waste heat without being put to practical use [4]. Recovering this massive amount of dumped thermal energy will improve the overall efficiency and sustainability in the field of power production [5]. To do so, it requires fine-tuning control and operating parameters [6–8]. Detailed monitoring of thermal processes in a plant is essential so that it is possible to know the places with the greatest energy loss and verify significant deviations from this thermal consumption. In a facility, it is the amount of energy from the primary source that was consumed without generating a profit for the company. According to Ramousse and Goupil [9], the various modes of operation also require a convenient analysis to evaluate the potential of the thermoelectric system as a function of the operating conditions.

Agarwal et al. [10], Costa and Sodré [11], Zhou et al. [12] and Tang et al. [13] demonstrated through their studies the importance of parameter adjustments of internal combustion engines and how this influences the efficiency of these engines. Both Payri et al. [14] and Lujan et al. [15] use in-cylinder pressure plus an encoder to diagnose ICE faults, but offline. Morey and Seers [16] also used in-cylinder pressure and an encoder but added exhaust gas measurement for a more accurate ICE diagnosis. Ahmadi et al. [17] and Kaushik et al. [18] presented studies on both the energetic and economic aspects of thermal power plants. From them, it is possible to understand how each subsystem influences the generation of a TPP and how better efficiency of these subsystems generates economic gains. In addition to economic gains, ICE with greater efficiency tends to generate less pollution, an increasingly requested requirement to preserve the environment. Leach et al. [19] and Konieczna et al. [20] show in their studies how the increase in efficiency can decrease the generated pollution.

To the best of the author's knowledge, there are very few studies in the literature (or none) that investigate both the in-cylinder pressure measurement part and the integration part of the other subsystems of this engine in order to perform an accurate diagnosis of the ICE. As a result, the purpose of this manuscript is to go further and accomplish this.

Therefore, this paper presents the monitoring of the operating condition (hence, the efficiency) of the Internal Combustion Engines (ICE) of TPPs mainly by analyzing the in-cylinder pressure curves, in order to detect problems associated with performance. The pressure curves are obtained with the system developed by the authors in Ref. [21], where pressure data is sent through Wi-Fi [22] to a remote computer running the analysis software. The presented technique aims at the operation with maximum efficiency of the ICE, also considering the injection phenomena, chemical reactions, radiation, conduction, lubrication, and cooling. The proposed approach, using these concepts, aims to provide the operator a visual interface through the use of the Sankey Diagram. This allows for an easy understanding of how the engine operating process is at all times and also allows the identification of which subsystem may be subtracting more or less energy from their process.

The rest of the article is organized as follows: Section 2 presents the fundamental concepts about the modeling of the powers and their use in the Sankey diagram. Section 3 presents the experimental results collected both in a controlled setup and in an actual TPP in Brazil. Finally, Section 4 presents the main conclusions of the study and some opportunities for future research.

2. Materials and Methods

The study was conducted at the Pernambuco III thermoelectric plant, located in the city of Igarassu-Pernambuco, Brazil, with a generation capacity of 200.79 MW, powered by heavy fuel oil (HFO), and consisting of 23 turbogenerator units (Diesel Engine 20V32 Wärtsila, as shown in Figure 1). This plant belongs to the Brazilian National Interconnected System (SIN) and is managed by the Brazilian Power System Operator ONS under a dispatch regime.

The main mechanical component of the plant is the internal combustion reciprocating engine [23] (Diesel Engine 20V32 Wärtsila), whose characteristics are presented in Table 1. In this sense, it is important to ensure the proper functioning of the operational components in the generation of electricity. Therefore, to achieve this objective, in the next subsections, the ICE components and subsystems (Section 2.1), the Sankey diagram (Section 2.2) and the complementary instrumentation (Section 2.3) for the measurements of the in-cylinder pressure will be described in detail. Finally, Section 2.4 presents the entire calculation process that went into developing the system.

Table 1. Basic characteristics of the Wärtsilä 20V32 GD diesel engine.

Diameter of cylinder (mm)	320
Course of cylinder (mm)	400
Volume of cylinder (m ³)	0.03217
Number of intake valves	2
Number of outtake valves	2
Number of cylinders	20
Engine speed/rotation (rpm)	750
Average speed of cylinders (m/s)	10
Average power per cylinder (kW)	580
Viscosity of fuel at 50 °C (cSt)	2-730

**Figure 1.** Diesel Engine 20V32 Wärtsilä.

2.1. Internal Combustion Engine Subsystems

In this subsection, all the basic components and subsystems of an ICE and how they influence the performance of these engines will be discussed. In total, the following components and subsystems will be presented:

- Injection system
- Lubrication system
- Cooling system
- Turbocharger system

The injection system is formed, basically, by the injectors and the pumping system. The injectors have aerothermodynamic formats for each type of fuel. The pumping system usually uses positive displacement pumps. The analysis of the fuel injection system is very important, as it uses energy taken from the generator to drive the fuel pumping system. In addition to these subsystems, the injection system contains a regulation and control subsystem based on the required torque, network frequency, and temperature of the cooling system [24]. A calibrated injection system ensures that the fuel is injected right at the moment of maximum compression, guaranteeing greater performance for the engine.

The second mechanical system to be described is the lubrication system. This system has the function of supplying protective oil to the sliding surfaces in order to reduce friction and cool them. Its operational principle is based on the movement of the lubricating oil produced by the gear pump. In addition to these subsystems, the lubrication system has heat exchangers and an oil pressure control system in order to ensure the maintenance of the lubricating oil. Proper lubrication helps to reduce friction losses away from the entire engine, thereby increasing the efficiency of the ICE.

The third mechanical system to be described is the cooling system. This system protects the engine from the rise in temperature during the combustion process. This rise in temperature is the result of friction between solid parts when there is a lack of lubrication. The cooling system guarantees acceptable temperatures to maintain the structural integrity

of the ICE block. All ICE has an optimal temperature point to guarantee maximum performance. It is the responsibility of the cooling system to ensure that the engine operates at a temperature close to this.

Finally, the last system analyzed for energy purposes is the turbocharger system. This system is comprised of turbines that provide shaft power from the energy of the exhaust gases. This shaft power is used to compress the air admitted to the combustion process through the compressor. A heat exchanger, commonly known as an intercooler, is used with the turbocharger system. This heat exchanger has the function of reducing the temperature of the inlet air, allowing a greater mass flow of air in the cylinder. In this subsystem, part of the energy from the exhaust gases that would be wasted is reused, which guarantees a considerable increase in engine efficiency.

2.2. Sankey Diagram

The portions of energy or power destined for each system that makes up the engine are accounted for by the Sankey thermodynamic diagram. The Sankey diagram for the case of the Diesel cycle engine under study is shown in Figure 2.

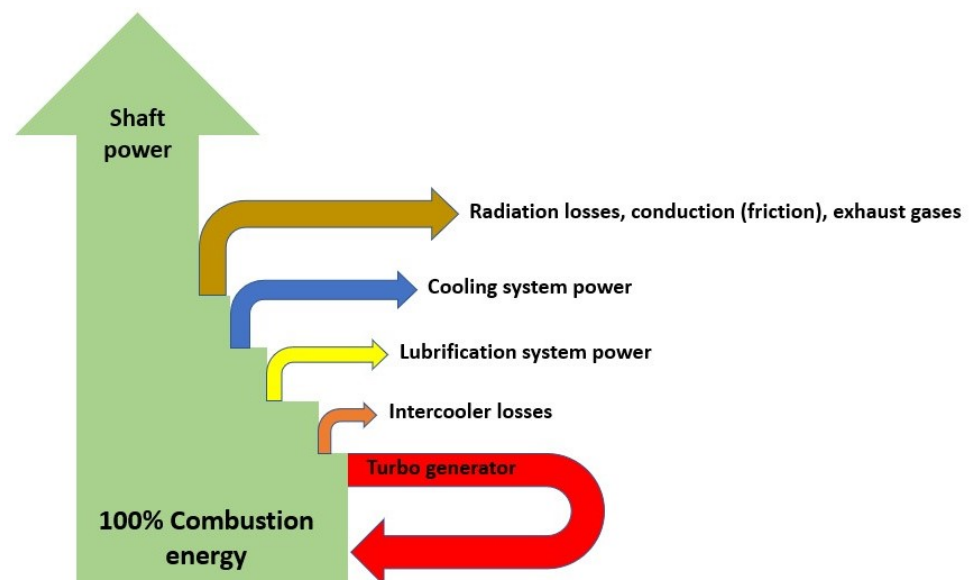


Figure 2. Sankey diagram for the Diesel engine.

The Sankey diagram is a type of diagram that, in the case of its use, helps in an easy and simple way to verify the energies lost during the combustion process, in addition, of course, to the useful energy available at the end of the combustion. With it, it is simple to evaluate each ICE subsystem and, through historical data, notice any abnormality in any subsystem.

To create the Sankey diagram, each main piece of equipment that composes the subsystems mentioned in the subsection was modeled. This equipment was modeled based on commonly measured values such as temperature, pressure, etc. The detailed procedure for modeling each subsystem is presented in Section 2.4. The data to feed the equations is obtained from a monitoring system developed by the authors in [21], which is described in the following subsection.

2.3. Complementary Instrumentation

An internal pressure monitoring system has been developed by the authors [21] in order to obtain precise information about the internal pressure. The system is mainly composed of in-cylinder pressure sensors (Section 2.3.1) and an instant speed of the crankshaft sensor (Section 2.3.2)-hence, the in-cylinder pressures can be obtained in relation to the rotation of the machine.

2.3.1. In-Cylinder Pressure Monitoring

The pressure sensors, whose photo is presented in Figure 3, allow for remote monitoring of the behavior of the combustion chamber pressure and temperature. Hence, it is possible to extract quantities such as compression pressure and combustion pressure in addition to temperatures. Such information allows estimating the volume of energy generated in the cylinder and how much of it is being effectively transformed into energy and, subsequently, allows identifying any possible failure in the engine.



Figure 3. In-cylinder pressure sensor developed in Ref. [21].

For sensor construction, a piezoresistive transducer (PA-7L), manufactured by Keller in Winterthur, Switzerland, was chosen. This sensor has a range of 0 to 200 bar ($\pm 0.5\%$), which is sufficient for measurements at both the TPP ICE (180 bar) and the reduced-size laboratory ICE (whose cylinder pressure is around 35 bar). Each pressure sensor in the proposed system communicates the recorded data to a distant computer running analytic software through WiFi connectivity. A microcontroller CC3200 [22] is used to enable WiFi functionality. This microcontroller is built around an ARM Cortex M4 core and has a 4-channel, 12-bit analog-to-digital converter (ADC). One of the ADC's channels gets data from a pressure transducer, while another channel receives data from a temperature transducer (also located inside the sensor housing). The temperature transducer's role is to compensate for pressure measurements. All in-cylinder pressure sensor readings must be synced to the same reference. As a result, each in-cylinder pressure sensor receives a sync signal from Section 2.3.2's encoder.

2.3.2. Instant Speed Monitoring

In order to monitor the instantaneous speed of the crankshaft (α), an incremental encoder (DFS60), manufactured by SICK was chosen. The encoder enables a measurement of 65,536 pulses per revolution with an uncertainty of $\pm 0.003^\circ$. Figure 4 shows the encoder. From this, it is possible to connect the information about the in-cylinder pressure to the physical instant of the piston in the cylinder. It is known that the evaluation of the compression pressure at the moment of the maximum upper point of the cylinder, a point known as the TDC (Top Dead Center), is essential to guarantee the maximum use of combustion energy. With the use of this principle, other energy gains can also be observed in detail by this remote measurement equipment.



Figure 4. Incremental Encoder DFS60-TDPA65536.

2.4. Calculation Procedure

Using the pressure data obtained with the in-cylinder sensors (Section 2.3.1) and crossing this information with the output of the encoder (Section 2.3.2), a P (Pressure) α (crankangle) curve is obtained, as illustrated in Figure 5. The red downward triangles represent the pressure acquisition points during the compression stroke of the piston, while the blue upward triangles represent the pressure points during the power stroke. The figure also indicates that the TDC takes place at $\alpha = 0^\circ$.

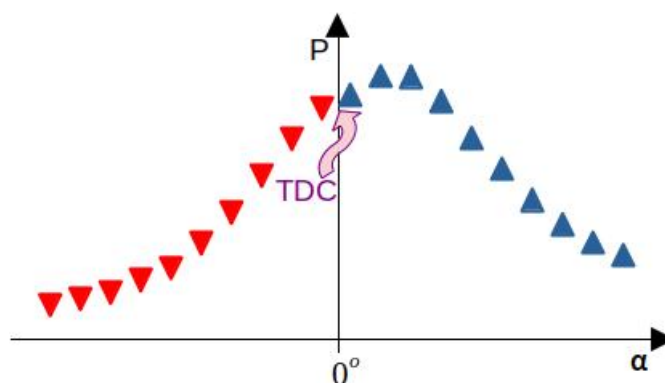


Figure 5. Concept of $P\alpha$ curve.

Considering the engine's construction parameters, the information about volume V can be obtained from the crankshaft angle α , as presented in Equation (1).

$$\begin{cases} V = \frac{1}{4} \cdot \pi \cdot D^2 \cdot e(\alpha), \\ e(\alpha) = \sqrt{l^2 - r^2 \cdot \sin^2 \alpha} + r \cdot \cos \alpha, \end{cases} \quad (1)$$

where $e(\alpha)$ is the piston stroke length as a function of the crankshaft angle α . D is the piston diameter, l is the connecting rod length, and r is the radius of the crankhandle.

Knowing the relationship between crankangle α and volume V , the acquired pressure points can be plotted as a function of V , on what is known as the PxV curve, as presented in Figure 6. Using the same convention as Figure 5, the red downward triangles represent the pressure acquisition points during the compression stroke, while the blue upward triangles represent the pressure points during the power stroke. Besides the TDC, the figure indicates where the BDC (Bottom Dead Center) takes place. The BDC is the lowest position of the piston (where the cylinder volume is at its maximum). The figure also presents a small area formed by the scavenging pressure P_{scav} (indicated with green stars). This area is usually small and can be disregarded.

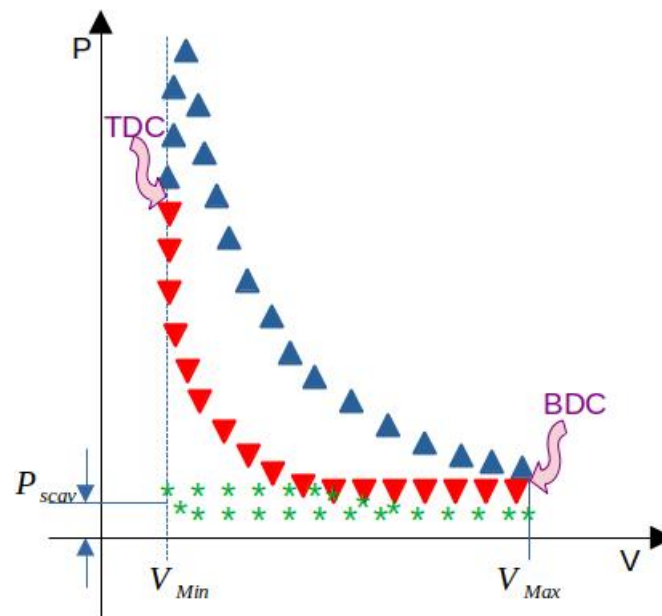


Figure 6. Concept of PxV curve—Based on [25].

Considering either Figure 5 ($Px\alpha$) or Figure 6 (PxV), the Mean Indicated Pressure (MIP) can be calculated as the average of the power stroke pressure points (blue upward triangles) subtracted by the average of the compression stroke pressure points (red downward triangles), as indicated in Equation (2).

$$MIP = \frac{1}{n_{pwr}} \cdot \sum_{k=1}^{n_{pwr}} P_{pwr}(k) - \frac{1}{n_{comp}} \cdot \sum_{k=1}^{n_{comp}} P_{comp}(k) \quad (2)$$

where n_{pwr} is the number of pressure points $P_{pwr}(k)$ acquired during the power stroke (at a given point k). n_{comp} is the number of pressure points $P_{comp}(k)$ acquired during the compression stroke. As the system acquires numerous cylinder pressure points that are synchronized with the crankshaft axis, it is sufficient to average the points pressure 180° to the left and right of the TDC (if the $Px\alpha$ curve is considered).

After calculating the MIP, the indicated power can be computed using Equation (3).

$$P_i = \frac{MIP \cdot V_{Max} \cdot n}{60 \cdot i}, \quad (3)$$

where V_{Max} is the maximum cylinder volume (obtained at the engine's manual) and n is the engine's rotation/speed (measured with the encoder). For the case of a 4-stroke engine, a correction factor $i = 2$ is used.

Once the indicated power is calculated, the effective power can be estimated using the mechanical efficiency of the engine, as indicated in Equation (4).

$$P_{ef} = P_i \cdot \eta_{engine}, \quad (4)$$

where η_{engine} is the efficiency of the engine (obtained from the engine's manual).

The effective power is the power at the shaft of the engine; in other words, it is the power that generates work and moves the electrical generator. Considering the Sankey diagram of Figure 2, the effective power is indicated by the main vertical arrow. For an engine without any losses, all input power (fuel power) would be converted in shaft power. For a practical engine, however, there are losses and powers that are consumed by the auxiliary subsystems (all of these are represented by the horizontal arrows in Figure 2 and are calculated in Sections 2.4.1–2.4.6).

The fuel power, which is the input to the Sankey diagram in Figure 2, can be estimated using the engine consumption data. Considering Wartsila engines, there is a fuel consump-

tion sensor whose information can be accessed from the WOIS database. Knowing the fuel consumption at a given cycle, the fuel power can be calculated as Equation (5).

$$P_{fuel} = \dot{m}_{fuel} \cdot LHV, \quad (5)$$

where \dot{m}_{fuel} is the fuel consumption and LHV is the Lower Heating Value of that particular fuel (which is obtained at certified laboratory tests).

2.4.1. Consumed Injection Power

The consumed injection power (P_{inj}) can be calculated using Equation (6).

$$P_{inj} = \dot{m}_{fuel} \cdot \frac{\Delta p}{\rho_{fuel}}, \quad (6)$$

where Δp is the pressure drop (obtained from the WOIS database in case of Wartsila engines) and ρ_{fuel} is the density of that particular fuel (which is obtained at certified laboratory tests).

2.4.2. Consumed Cooling Power

The consumed cooling power (P_{cool}) can be calculated using Equation (7).

$$P_{cool} = \dot{V}_{wtr} \cdot \Delta p, \quad (7)$$

where \dot{V}_{wtr} is the volumetric flow of the cooling water (obtained from the WOIS database in case of Wartsila engines).

2.4.3. Consumed Lubrication Power

The consumed lubrication power (P_{lub}) can be calculated using Equation (8).

$$P_{lub} = \dot{V}_{oil} \cdot \Delta p, \quad (8)$$

where \dot{V}_{oil} is the volumetric flow of the lubricating oil (obtained from the WOIS database in the case of Wartsila engines).

2.4.4. Dissipated Heat

Two main powers due to dissipated heat are considered here: the dissipated heat at the cooling system ($P_{coolHeat}$, calculated using Equation (9)) and the dissipated heat at the lubrication system ($P_{lubHeat}$, calculated using Equation (10)). The sum of these two results in the total dissipated heat ($P_{TotalHeat}$), as presented in Equation (11).

$$P_{coolHeat} = \dot{V}_{wtr} \cdot \rho_{wtr} \cdot C_{wtr} \cdot (T_{wtrIn} - T_{wtrOut}), \quad (9)$$

where $\rho_{wtr} = 997 \text{ kg/m}^3$ is the density of water and $C_{wtr} = 4.19 \text{ kJ/kg}$ is the heat capacity of water. T_{wtrIn} and T_{wtrOut} are, respectively, the inlet and outlet water temperatures (which are obtained from the WOIS database in case of Wartsila engines).

$$P_{lubHeat} = \dot{V}_{oil} \cdot \rho_{oil} \cdot C_{oil} \cdot (T_{oilIn} - T_{oilOut}), \quad (10)$$

where ρ_{oil} and C_{oil} are, respectively, the density and the heat capacity of lubricating oil (both obtained from laboratory tests). T_{oilIn} and T_{oilOut} are, respectively, the inlet and outlet lubricating oil temperatures (which are obtained from the WOIS database in the case of Wartsila engines).

$$P_{TotalHeat} = P_{coolHeat} + P_{lubHeat}. \quad (11)$$

2.4.5. Turbocharger Power

The re-used turbocharger power can be obtained using Equation (12).

$$P_{turbocomp} = \dot{m}_{air} \cdot C_{air} \cdot (T_{airIn} - T_{airOut}), \quad (12)$$

where \dot{m}_{air} is the mass flow of the inlet air (obtained from the WOIS database in case of Wartsila engines). $C_{air} = 1.012 \text{ kJ}/(\text{kg} \cdot \text{K})$ is the specific heat of the inlet air. T_{airIn} and T_{airOut} are, respectively, the inlet and outlet temperatures of the air (which are obtained from the WOIS database in the case of Wartsila engines).

2.4.6. Other Consumed Power

All other sources of consumed power not calculated in Sections 2.4.1–2.4.5, such as friction, radiation, etc., can be grouped in a category called “others”. These other powers can be obtained as the difference between fuel power (P_{fuel} , the input to the system), effective power (P_{ef} , the power that generates useful work at the shaft), and the sum of the previously discussed losses, as presented in Equation (13).

$$P_{others} = P_{fuel} - P_{ef} - P_{inj} - P_{rfr} - P_{lub} - P_{TotalThrmI} - P_{turbocomp}. \quad (13)$$

3. Results and Discussion

This section presents both the results obtained in the model at a reduced scale and those obtained in the Pernambuco III thermal power plant. In the reduced scale model, it was studied how to identify faults in ICE through the $Px\alpha$ and PxV curves and also how these defects influence the generation. In Pernambuco III, the in-cylinder pressure monitoring system was added to the developed supervisory system. The developed supervisor uses in-cylinder pressure sensors and data from the WOIS database (i.e., fuel consumption, volumetric flow of the cooling water, volumetric flow of the lubrication oil, mass flow of the inlet air, and air temperatures) to perform the calculations of the Sankey diagrams (according to the procedure in Section 2.4, Equations (4)–(13)).

3.1. Results at the Reduced Scale Laboratory

The experiments in this subsection have been performed in the reduced-scale laboratory proposed by the authors in Ref. [21]. This is a controllable setup where malfunctions can be inserted on purpose in order to test equipment and algorithms for the detection of failures. Figure 7 presents the reduced scale laboratory, which is based on a Cummins C90D6B Diesel Generator. The goal of the tests is to compare the $Px\alpha$ and PxV curves of the engine in normal condition and in a failure condition.

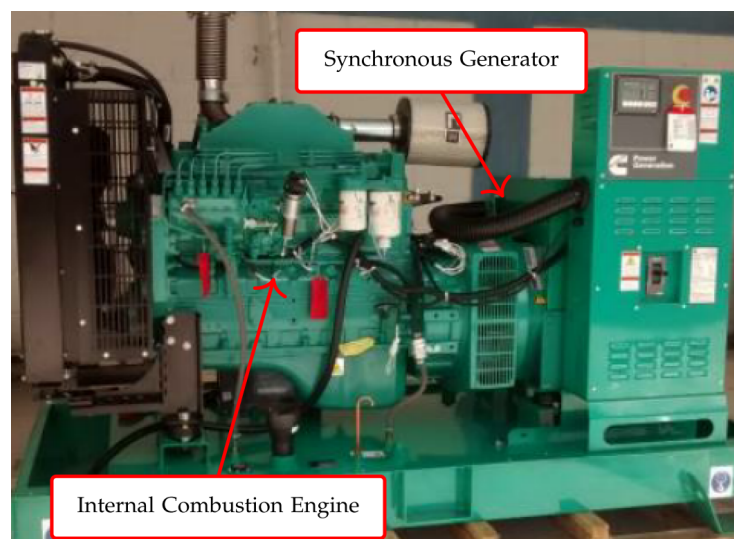


Figure 7. Reduced scale laboratory with a Cummins C90D6B Diesel Generator, extracted from [21].

The ICE part of the Cummins C90D6B group generator has a total of six cylinders, but only four were monitored in the tests. Figure 8 presents the engine injection pump. By changing its position, it is possible to delay or advance the injection of fuel into the injection chamber, which consequently generates an undesirable operating condition. The electrical part of the generator group is connected to two constant loads of 24 kW.



Figure 8. Injection pump at the ICE.

Two tests were performed: the first with the fuel injection pump out of adjustment and the second with the fuel pump in the regulated position. In order to perform the tests, a fuel tank separate from the engine was used. In this tank, a volume of 5 L was measured using a beaker (as presented in Figure 9) for the two tests. The beaker has a measurement uncertainty of ± 10 mL. A maximum time of 20 min for the engine to run was also stipulated. At the end of the time, the remaining volume of fuel was measured again using the beaker.



Figure 9. Beaker with the fuel oil for the tests.

A Fluke 435 Series II instrument was used in order to measure the electrical energy generated. The Fluke 435 Series II has a measurement uncertainty of $\pm 1\%$ for kWh. During the entire process of engine operation in both conditions, several signals of the internal pressure of the monitored cylinders were acquired through the installed sensors.

Table 2 presents the generated electrical energy and the fuel consumption for both test conditions. The results clearly show that with the unregulated pump, there is less energy generated in addition to an increase in fuel consumption.

Table 2. Fuel consumption and electrical energy generated at both engine conditions.

Test Condition of Fuel Injection Pump	Fuel Consumption	Generated Energy
out of adjustment	3920 mL	7.170 kWh
regulated position	3650 mL	7.304 kWh

From this result, it is sought through the $Px\alpha$ and PxV curves to find evidence that demonstrates the failure condition. For this comparison, only the signals from cylinder 1 will be used, although the analysis for the other cylinders occurs in a similar way.

Figure 10 presents the $Px\alpha$ curve of cylinder 1 for the two test conditions. The pink curve represents the regulated pump condition and the blue curve the unregulated pump condition. Analyzing the curves, it is clear that the curve of the regulated pump has higher compression and explosion pressure. In addition, it can be noted that a better defined compression region can be found, since in the faulty curve it is very difficult to differentiate the compression region from the explosion region. These factors indicate that the explosion of the blue curve is happening the wrong way; that is, it is not happening in the TDC. This defect can be seen in the shape of the pressure curve, the maximum pressures of the cycle, and the engine's efficiency. The pressure curves also show that the compression region is angularly out of phase with the TDC (0° for cylinder 1). It is likely that with an adjustment of the engine, this delay can be adjusted and, as a result, the efficiency of the engine can be increased.

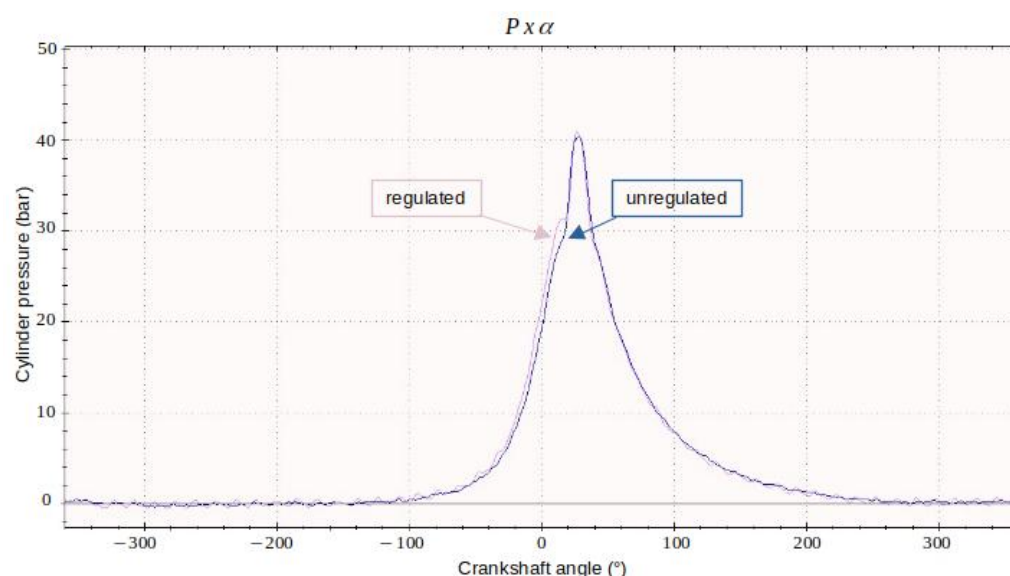


Figure 10. $Px\alpha$ curve of cylinder 1 for the test conditions of injection pump.

Figure 11 presents the PxV curve of the condition with an unregulated pump, and Figure 12 presents the PxV curve of the regulated pump condition. Analyzing the curves comparatively, the unregulated pump curve has a lower pressure at the lowest volume point, that is, the TDC. In addition, a larger explosion region is observed compared to the no-defect curve. Another way of evaluating the cycle's performance would be through

the internal area of the cycle. Hence, visually, it is difficult to assess which cycle has a larger area than the other. Hence, the MIP of the curves is calculated as presented in the procedure of Section 2.4, using Equation (2). Table 3 presents the calculated value of MIP for each cylinder at each test condition of the injection pump. The computed data show that the regulated engine has a greater MIP and, as a result, a higher output power. Only cylinder 4 exhibited a higher MIP in the unregulated condition, indicating that in the regulated condition it is not the most feasible configuration, leaving gaps for increases in the engine's performance.

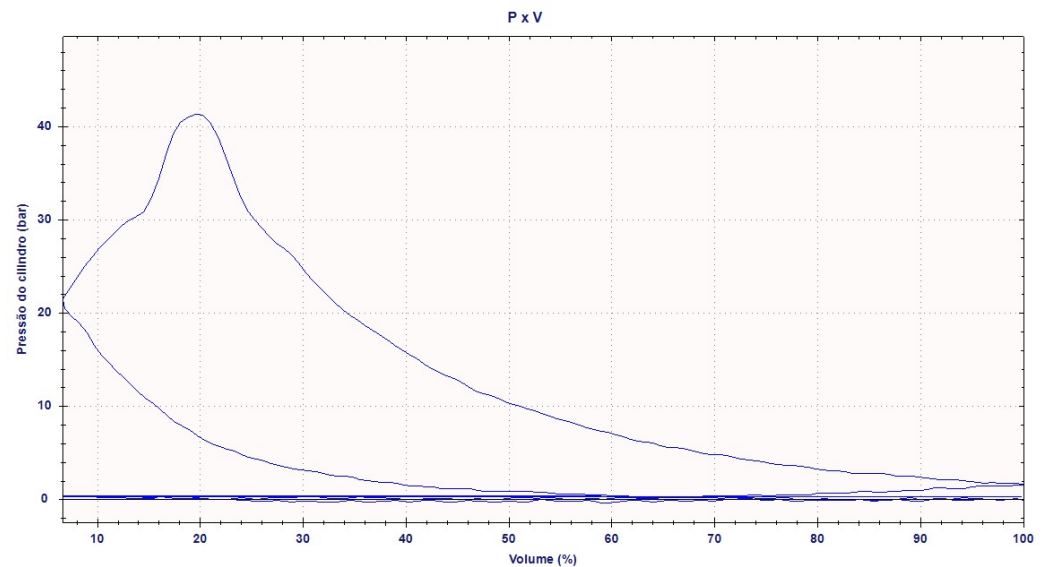


Figure 11. PxV curve of cylinder 1 for the test condition of unregulated injection pump.

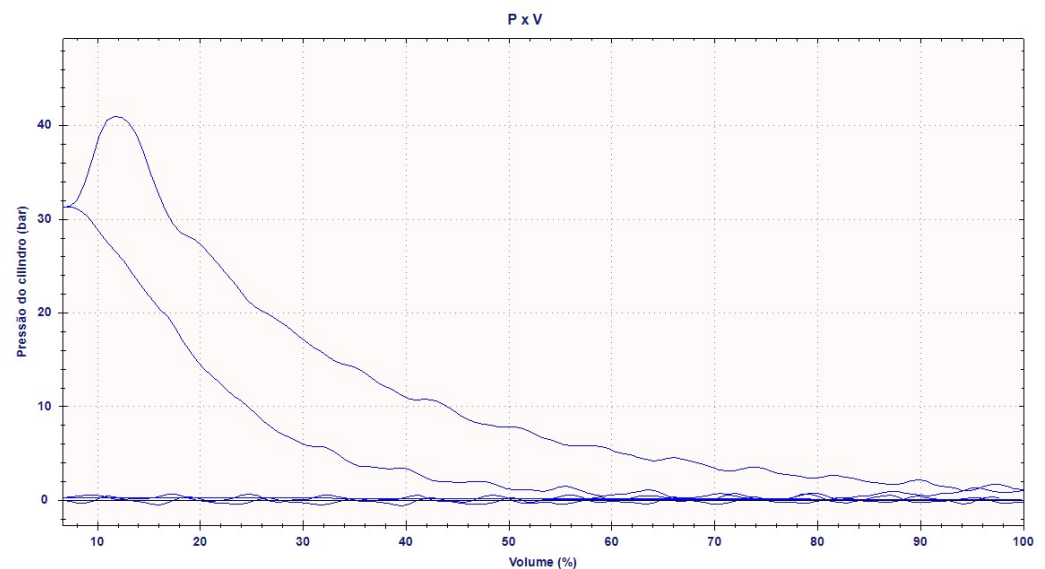


Figure 12. PxV curve of cylinder 1 for the test condition of regulated injection pump.

Table 3. MIP for each cylinder at each test condition of the injection pump.

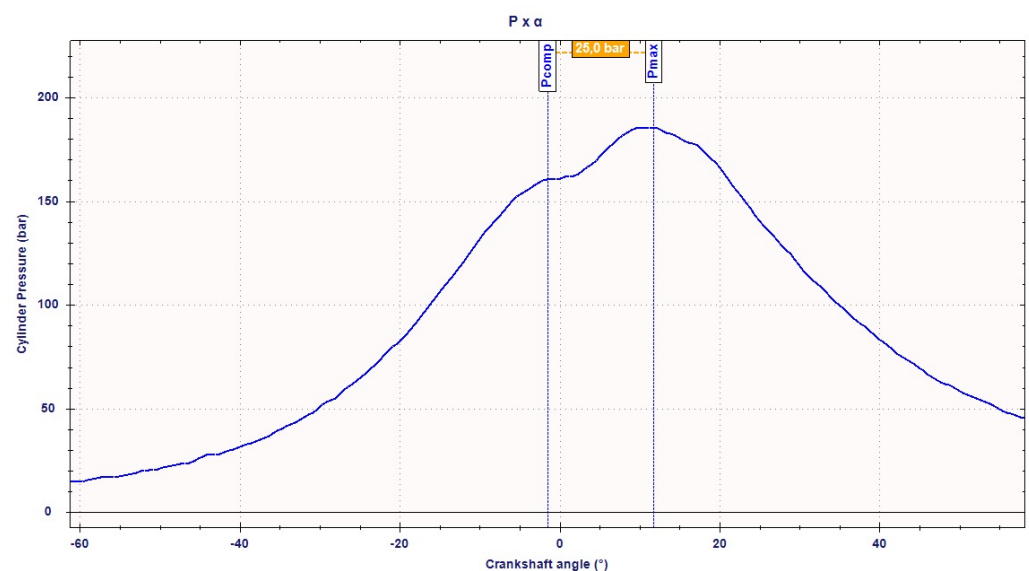
Cylinder (Test Condition)	MIP
Cylinder 1 (unregulated pump)	8.4 bar
Cylinder 2 (unregulated pump)	7.6 bar
Cylinder 3 (unregulated pump)	9.3 bar
Cylinder 4 (unregulated pump)	7.9 bar
Cylinder 1 (regulated pump)	8.6 bar
Cylinder 2 (regulated pump)	8.1 bar
Cylinder 3 (regulated pump)	9.4 bar
Cylinder 4 (regulated pump)	7.8 bar

From the results above, it was possible to demonstrate that from the $Px\alpha$ and PxV curves and also by the MIP, it is possible to identify failures in internal combustion engines. However, only $Px\alpha$ and PxV curves can be used to pinpoint the location of the failure; that is, only the presence of a failure can be identified. It is necessary to combine the information from the curves with other information, such as inlet mass flow, to identify which subsystem is at fault.

3.2. Results at the Pernambuco III Power Plant (Brazil)

The experiments in this subsection have been performed at the Pernambuco III thermolectric plant, located in the city of Igarassu, Brazil. This plant has a generation capacity of 200.79 MW and is powered by 23 turbogenerator units with Wartsila 20V32 ICEs. Here, in contrast to the previous subsection (where failures could be inserted on purpose), the regular operation of the plant is presented.

Figure 13 presents the $Px\alpha$ curve for one of the cylinders of the engine of generation unit #22. It can be seen that the compression is quite near the TDC (which happens at the 0° angle), indicating that the valves are well adjusted. Furthermore, it can be seen that the explosion of the fuel results in a pressure rise of 25 bar. According to the engine's manual, which is the nominal operation of the engine; if, however, the difference was less, that would indicate a loss of efficiency.

**Figure 13.** $Px\alpha$ curve of 1 of the 20 cylinders of Engine #22 of the Pernambuco III plant.

From the procedure of Section 2.4, the MIP of the pressure points on the curve of Figure 13 can be calculated using Equation (2), resulting in $MIP = 27.8$ bar.

Knowing the value of the MIP, the maximum cylinder volume (expressed in Table 1 as $V_{Max} = 0.03217 \text{ m}^3$) and the engine speed (measured with the encoder as $n = 720 \text{ rpm}$), the indicated power can be computed using Equation (3) as $P_i = 537 \text{ kW}$.

Once the indicated power is calculated, the effective power can be calculated using Equation (4), as $P_{ef} = 429 \text{ kW}$ (considering a mechanical efficiency of $\eta_{engine} = 0.80$, from the engine's manual).

The fuel power can be calculated using the engine consumption data. From Wartsila's WOIS database, a fuel consumption of $\dot{m}_{fuel} = 0.02486 \text{ kg/s}$ (for one cylinder) has been measured for that given cycle. Considering that the Lower Heating Value for that particular fuel (obtained at a certified laboratory test hired by Pernambuco III thermal power plant) is $LHV = 41,500 \text{ kJ/kg}$, using Equation (5), the fuel power (for one cylinder) can be calculated as $P_{fuel} = 1075 \text{ kW}$. This same process is repeated for the remaining 19 cylinders. Applying the procedure of Section 2.4, the powers and losses for each subsystem are calculated and the developed software plots the Sankey diagram. Figure 14 presents the Sankey diagram for engine #22, with data from 9 June 2022.

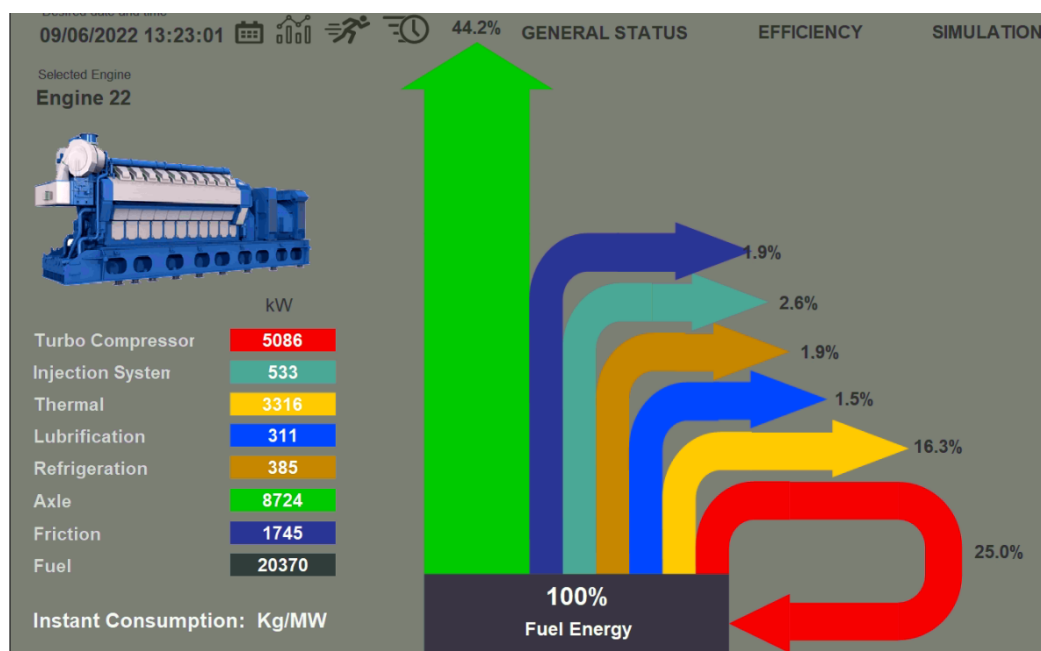


Figure 14. Capture of the developed analysis software, presenting the Sankey diagram of engine #22, on 9 June 2022.

Of the 23 generating units at the plant, 20 will have the proposed system installed. The proposition of the developed tool is the comparison of the efficiencies and losses of the engines in order to determine which of the units present opportunities for adjustments in settings and operational points. This plant is operated within an energy dispatch model, hence, it remains idle for a large portion of the year and is operational only during the drought season (when the cost of hydro power is increased). So far, only unit #22 has had the in-cylinder pressure sensors installed (for a quick test with the results presented above). In order to check the feasibility of the proposed software, data from the WOIS database from January 2020 has been used.

The same procedure as in Section 2.4 has been used in order to obtain the Sankey diagrams below.

The only exception was the effective power, which was obtained from the generated electrical power (P_{el} , from the WOIS database) divided by the efficiency of the electric generator ($\eta_{generator}$, from the generator's manual), as in Equation (14). However, in this way, the accuracy is compromised since the efficiency of the generator decreases over time, causing it to be considered to have an efficiency greater than the real one. It is important

to note that the data from the electric generator has been used only because the pressure sensors were not installed at that time. Figures 15–17 present the Sankey diagrams of engines #04, #11, and #17, respectively.

$$P_{ef} = \frac{P_{el}}{\eta_{generator}} \quad (14)$$

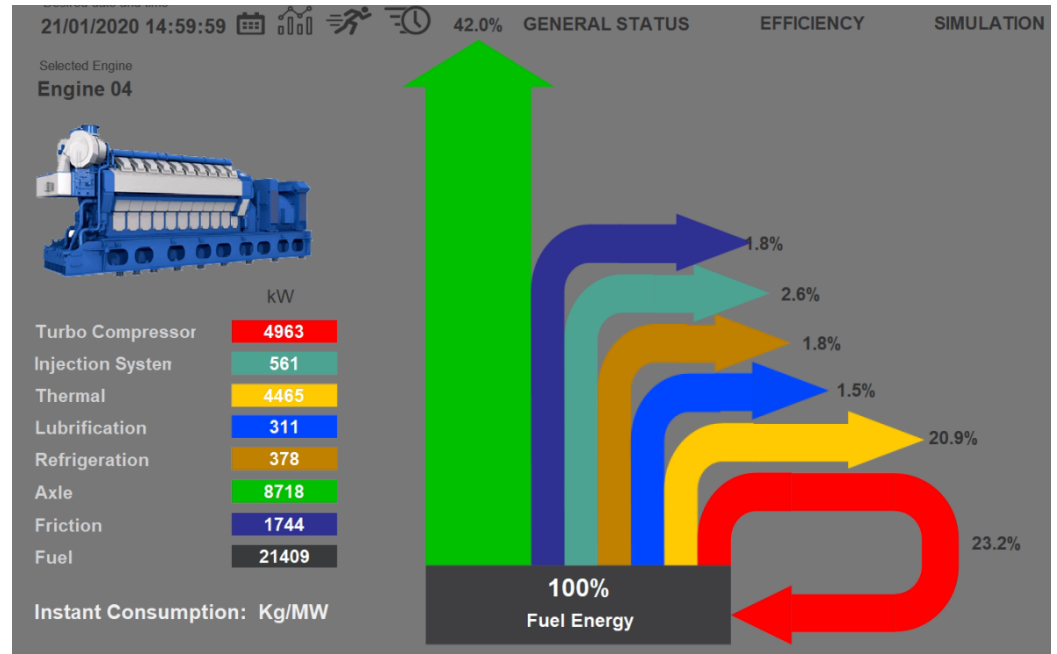


Figure 15. Capture of the developed analysis software, presenting the Sankey diagram of engine #04, on 21 January 2020.

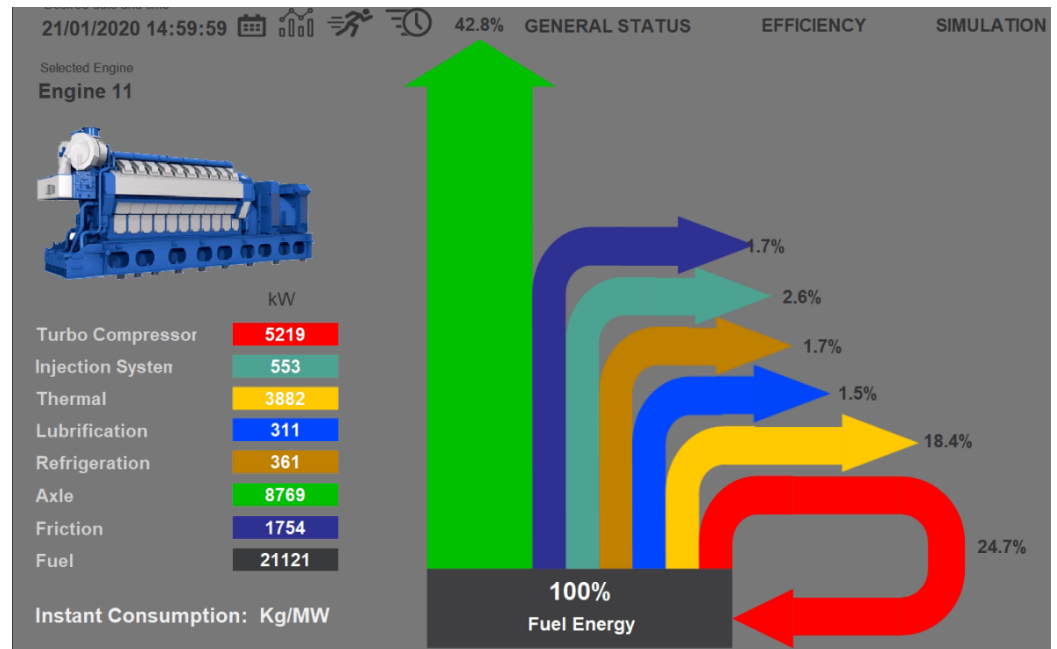


Figure 16. Capture of the developed analysis software, presenting the Sankey diagram of engine #11, on 21 January 2020.

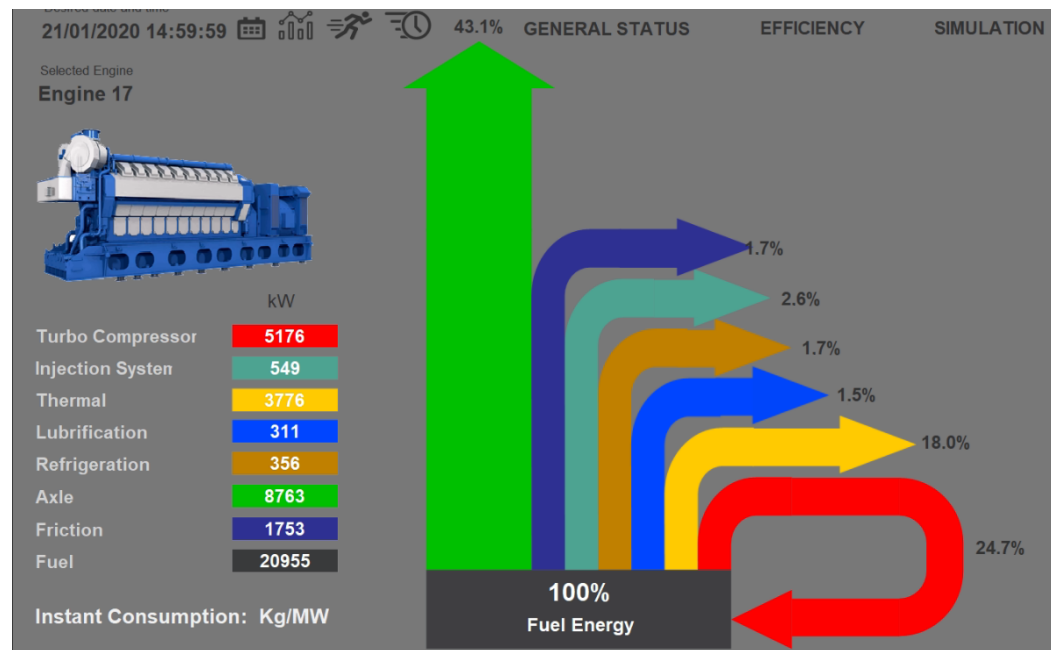


Figure 17. Capture of the developed analysis software, presenting the Sankey diagram of engine #17, on 21 January 2020.

Figure 18 was created in order to simplify the comparison between engines. In it, it is possible to clearly see the differences between the subsystems of each engine, highlighting abnormal conditions. For this, the graph uses the lowest percentage value of the 3 engines for each subsystem as a base and presents the difference between the base and the other engines. By comparing engines #4 (Figure 15), #11 (Figure 16), and #17 (Figure 17), it can be seen that for the injection, lubrication, refrigeration, and friction subsystems, there are very similar values between them. This indicates that there is no abnormality in these subsystems. However, for engine #4, there is a large value of thermal loss compared to the other two engines. This thermal loss is reflected in a lower use of energy from the turbo compressor system, and consequently, we have a lower shaft power. With this information, it is possible to identify the exact location of the problem, reducing the time and cost of engine maintenance, in addition to ensuring greater performance. For power generation scenarios, such as the case studied, small differences in engine efficiency, when accumulated over hours of operation (considering elevated volumes of fuel consumed), result in significant economic gains that should be explored in control and scheduled maintenance. This same analysis could be done for the other subsystems and with a greater number of machines. The developed supervisory system has a number of information sources. The greater the number of sources, the better the maintenance planning and, consequently, the efficiency of the thermal power plant.

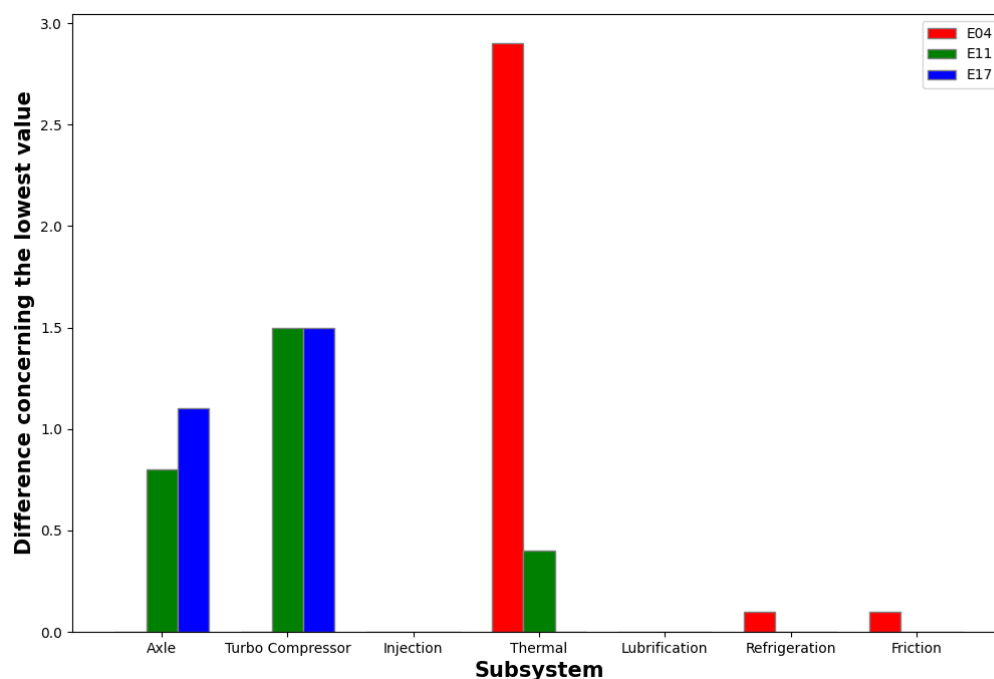


Figure 18. Comparison between the engine subsystems.

4. Conclusions and Future Work

This work presented a system to identify failures and evaluate the efficiency of the different subsystems of ICEs of TPPs. This information can be used by the TPP operators in order to adjust settings and operational points, as well as carry out more effective maintenance planning. The results are verified through two different setups: in a controlled laboratory, where failures were inserted on purpose, and at an actual TPP in Brazil.

The controlled test indicated that the proposed in-cylinder measurement system was able to detect the insert failure. In addition, at the actual TPP, the comparison of the Sankey diagrams of the monitored ICEs has pointed out that one engine could have adjustments on the thermal losses that influence the energy reuse of the turbo compressor system and consequently lower shaft power. In this way, it is possible to plan the maintenance exactly in the region that has the fault and recover the engine's performance.

It is important to note that even small differences in the efficiency of the subsystems, when accumulated over hours of operation, may result in significant economic gains for the TPP. In addition to economic gains, with increased efficiency, the emission of polluting gases can be reduced.

So far, as the TPPs in Brazil produce energy in a dispatch model, mostly when the cost of hydroelectric power is increased during the drought season of the year, the in-cylinder pressure system has been tested only in 1 of the 23 generation units of the Pernambuco III plant. For future work, it is expected to collect data from more engines during full-power operation. In addition, with the system collecting data for months of operation, the suggested adjustments to the subsystems are expected to result in significant energy savings for the plant.

Author Contributions: Conceptualization, L.C.R., H.F.V.-N., E.L.B. and F.d.O.A.; Data curation, E.L.B., G.L.-T. and P.G.P.d.M.; Formal analysis and Investigation, R.F.R.J., C.E.T., L.C.R., H.F.V.-N., E.L.B., L.E.d.L.d.O., F.d.O.A. and P.G.P.d.M.; Methodology and Software, L.C.R., E.L.B., L.E.d.L.d.O., G.L.-T., F.d.O.A., R.F.R.J., C.E.T. and P.G.P.d.M.; Writing, L.C.R. and W.C.S. All authors have read and agreed to the published version of the manuscript.

Funding: This research received no external funding.

Institutional Review Board Statement: Not applicable.

Informed Consent Statement: Not applicable.

Data Availability Statement: Not applicable.

Acknowledgments: The authors would like to thank UTE Pernambuco III and the Brazilian Research Agencies CNPq, CAPES and ANEEL R&D for their support of this project. The authors would also like to thank Luiz Eduardo Borges-da-Silva, Haylemar de Nazaret Cardenas-Rodriguez, Fernanda Mitchellly Vilas-Boas from Gnarus Institue and also Bruno Raphael Inocencio and Vitor Chaves Braga from Pernambuco III thermal power plant for occasional assistance in the preparation of the manuscript.

Conflicts of Interest: The authors declare no conflict of interest.

Abbreviations

The following abbreviations are used in this manuscript:

ANEEL	Brazilian Regulatory Agency for Energy
GD	Gas–Diesel
BDC	Bottom Dead Center
HFO	Heavy Fuel Oil
ICE	Internal Combustion Engine
LHV	Lower Heating Value
MIP	Mean Indicated Pressure
ONS	Brazilian Power System Operator
P	Pressure
PROCEL	Brazilian Program for Conservation of Electrical Energy
SIN	Brazilian National Interconnected System
TDC	Top Dead Center
TPP	Thermal Power Plant
V	Volume
WHR	Waste Heat Recovery
WOIS	Wärtsilä Operator’s Interface System

References

1. Santos, A.Q.; da Silva, A.R.; Ledesma, J.J.; de Almeida, A.B.; Cavallari, M.R.; Junior, O.H. Electricity Market in Brazil: A Critical Review on the Ongoing Reform. *Energies* **2021**, *14*, 2873. [[CrossRef](#)]
2. ANEEL. Sistemas de Geracao da ANEEL-SIGA. Available online: <https://www.gov.br/aneel/pt-br/centrais-de-conteudos/relatorios-e-indicadores/geracao#:~:text=SIGA%20%2D%20Sistema%20de%20Informa%C3%A7%C3%B5es%20de,reduzida%20com%20registro%20na%20Ag%C3%Aancia> (accessed on 6 June 2022).
3. Campos, M.M.; Borges-da-Silva, L.E.; Arantes, D.D.; Teixeira, C.E.; Bonaldi, E.L.; Lambert-Torres, G.; Ribeiro Junior, R.F.; Krupa, G.P.; Sant’Ana, W.C.; Oliveira, L.E.; et al. An Ultrasonic-Capacitive System for Online Characterization of Fuel Oils in Thermal Power Plants. *Sensors* **2021**, *21*, 7979. [[CrossRef](#)] [[PubMed](#)]
4. Forman, C.; Muritala, I.K.; Pardemann, R.; Meyer, B. Estimating the global waste heat potential. *Renew. Sustain. Energy Rev.* **2016**, *57*, 1568–1579. [[CrossRef](#)]
5. Mehmood, M.U.; Cho, S. Optimization of a Thermomagnetic Heat Engine for Harvesting Low Grade Thermal Energy. *Energies* **2021**, *14*, 5768. [[CrossRef](#)]
6. Gonzalez-Ayala, J.; Guo, J.; Medina, A.; Roco, J.; Hernández, A.C. Energetic self-optimization induced by stability in low-dissipation heat engines. *Phys. Rev. Lett.* **2020**, *124*, 050603. [[CrossRef](#)]
7. Gonzalez-Ayala, J.; Medina, A.; Roco, J.; Calvo Hernández, A. Thermodynamic optimization subsumed in stability phenomena. *Sci. Rep.* **2020**, *10*, 14305. [[CrossRef](#)]
8. Gonzalez-Ayala, J.; Guo, J.; Medina, A.; Roco, J.; Hernández, A.C. Optimization induced by stability and the role of limited control near a steady state. *Phys. Rev. E* **2019**, *100*, 062128. [[CrossRef](#)]
9. Ramousse, J.; Goupil, C. Chart for Thermoelectric Systems Operation Based on a Ternary Diagram for Bithermal Systems. *Entropy* **2018**, *20*, 666. [[CrossRef](#)]
10. Agarwal, A.K.; Srivastava, D.K.; Dhar, A.; Maurya, R.K.; Shukla, P.C.; Singh, A.P. Effect of fuel injection timing and pressure on combustion, emissions and performance characteristics of a single cylinder diesel engine. *Fuel* **2013**, *111*, 374–383. [[CrossRef](#)]
11. Costa, R.C.; Sodré, J.R. Compression ratio effects on an ethanol/gasoline fuelled engine performance. *Appl. Therm. Eng.* **2011**, *31*, 278–283. [[CrossRef](#)]
12. Zhou, Y.; Tang, J.; Zhang, C.; Li, Q. Thermodynamic analysis of the air-cooled transcritical Rankine cycle using CO₂/R161 mixture based on natural draft dry cooling towers. *Energies* **2019**, *12*, 3342. [[CrossRef](#)]

13. Tang, J.; Zhang, Q.; Zhang, Z.; Li, Q.; Wu, C.; Wang, X. Development and performance assessment of a novel combined power system integrating a supercritical carbon dioxide Brayton cycle with an absorption heat transformer. *Energy Convers. Manag.* **2022**, *251*, 114992. [[CrossRef](#)]
14. Payri, F.; Luján, J.M.; Martín, J.; Abbad, A. Digital signal processing of in-cylinder pressure for combustion diagnosis of internal combustion engines. *Mech. Syst. Signal Process.* **2010**, *24*, 1767–1784. [[CrossRef](#)]
15. Luján, J.M.; Bermúdez, V.; Guardiola, C.; Abbad, A. A methodology for combustion detection in diesel engines through in-cylinder pressure derivative signal. *Mech. Syst. Signal Process.* **2010**, *24*, 2261–2275. [[CrossRef](#)]
16. Morey, F.; Seers, P. Comparison of cycle-by-cycle variation of measured exhaust-gas temperature and in-cylinder pressure measurements. *Appl. Therm. Eng.* **2010**, *30*, 487–491. [[CrossRef](#)]
17. Ahmadi, M.H.; Alhuyi Nazari, M.; Sadeghzadeh, M.; Pourfayaz, F.; Ghazvini, M.; Ming, T.; Meyer, J.P.; Sharifpur, M. Thermodynamic and economic analysis of performance evaluation of all the thermal power plants: A review. *Energy Sci. Eng.* **2019**, *7*, 30–65. [[CrossRef](#)]
18. Kaushik, S.C.; Reddy, V.S.; Tyagi, S.K. Energy and exergy analyses of thermal power plants: A review. *Renew. Sustain. Energy Rev.* **2011**, *15*, 1857–1872. [[CrossRef](#)]
19. Leach, F.; Kalghatgi, G.; Stone, R.; Miles, P. The scope for improving the efficiency and environmental impact of internal combustion engines. *Transp. Eng.* **2020**, *1*, 100005. [[CrossRef](#)]
20. Konieczna, A.; Roman, K.; Borek, K.; Grzegorzewska, E. GHG and NH₃ Emissions vs. Energy Efficiency of Maize Production Technology: Evidence from Polish Farms; a Further Study. *Energies* **2021**, *14*, 5574. [[CrossRef](#)]
21. Assuncao, F.D.O.; Borges-da-Silva, L.E.; Villa-Nova, H.F.; Bonaldi, E.L.; Oliveira, L.E.L.; Lambert-Torres, G.; Teixeira, C.E.; Sant’Ana, W.C.; Lacerda, J.; da Silva Junior, J.L.M.; et al. Reduced Scale Laboratory for Training and Research in Condition-Based Maintenance Strategies for Combustion Engine Power Plants and a Novel Method for Monitoring of Inlet and Exhaust Valves. *Energies* **2021**, *14*, 6298. [[CrossRef](#)]
22. Texas Instruments. CC3200 Simple-Link Wi-Fi and Internet-of-Things Solution, a Single Chip Wireless MCU Technical Reference Manual. Available online: <https://www.ti.com/lit/ug/swru367d/swru367d.pdf> (accessed on 6 June 2022).
23. Niemi, S. Survey of Modern Power Plants Driven by Diesel and Gas Engines. 1997. Available online: <https://www.osti.gov/etdeweb/biblio/628799> (accessed on 6 June 2022).
24. Ogasawara, H.; Takai, M. Fuel Injection Timing Control System for a Diesel Engine. U.S. Patent US 4,388,909, 21 July 1983.
25. Jankowski, A.; Kowalski, M. Environmental Pollution Caused by a Direct Injection Engine. *J. Kones* **2015**, *22*. [[CrossRef](#)]